Design and development of a nozzle-free electrospinning device for the high-throughput production of biomaterial nanofibers

Muhammad Waqas*, Antonios Keirouz*, Maria Kana Sanira Putri, Faraz Fazal, Francisco Javier Diaz Sanchez, Dipa Ray, Vasileios Koutsos, and Norbert Radacsi†

School of Engineering, Institute for Materials and Processes, The University of Edinburgh, Robert Stevenson Road, Edinburgh, EH9 3FB, United Kingdom.

*These authors contributed equally to the article

†Corresponding author. Tel.: +44 (0) 131 651 7112. E-mail address: n.radacsi@ed.ac.uk

Abstract

This technical note provides a step-by-step guide for the design and construction of a temperature-controlled nozzle-free electrospinning device. The equipment uses a rotating mandrel partially immersed within a polymer solution to produce fibers in an upward motion by inducing the formation of multiple Taylor cones and subsequently multi-jetting out of an electrified open surface. Free-surface electrospinning can overcome limitations and drawbacks associated with single and multi-nozzle spinneret configurations, such as low yield, limited production capacity, nonuniform electric field distribution, and clogging. Most importantly, this lab-scaled high-throughput device can provide an alternative economical route for needleless electrospinning research, in contrast to the high costs associated with industrially available upscaling equipment. Among the device's technical specifications, a key feature is a cryo-collector mandrel, capable of collecting fibers in sub-zero temperatures, which can induce ultra-porous nanostructures, wider pores, and subsequent in-depth penetration of cells. A multi-channel gas chamber allows the conditioning of the atmosphere, temperature, and airflow, while the chamber's design averts user exposure to the high-voltage components. All the CAD files and point-by-point assembly instructions, along with a list of the materials used, are provided.

Highlights:

A step-by-step guide for the design and development of a cost-effective, high-throughput free-surface electrospinning device.

- The nozzle-free electrospinning device is capable of producing fibres in the micro/nanoscale. Random and aligned nanofibres mats can be produced at low and high revolution of collector respectively.
- Cryo-electrospinning is feasible through a special cylinder collector assembly, which can significantly increase the pore size and porosity of the developed nanofibrous scaffolds.
- Three variants of the spinneret assembly; a cylinder, a ball, and a spiral coil can accommodate different solution volumes and large-scale production of nanofibres, as the free-surface electrode has no clogging issues, and it allows the formation of multiple Taylor cones throughout its surface.
- A multi-channel gas chamber allows the conditioning of the atmosphere, temperature, and airflow, which has a direct effect in adjusting the solvent evaporation rate. The design of the chamber ensures that there is no exposure of the user to the high-voltage components.

1 Introduction

The unique properties presented by fibrous materials in the nano/microscale have directed the advancement of several fiber-processing techniques today. Among them, including thermal-induced phase separation, drawing, template synthesis, and self-assembly, electrospinning is of considerable significance as a rapidly evolving fiber preparation method (1). As a highly versatile method, electrospinning can process solutions, suspensions, or melts into fibers of varying diameters with low standard deviation (low polydispersity) and is the only process, at present, capable of mass-producing continuous nanofibers (NFs) (2, 3).

Electrospun NFs offer unique properties due to their high surface-to-volume ratio, fiber-length-to-diameter aspect ratio, and porosity (generally $\geq$ 70%) (4). The NFs produced can be tuned to present variant configurations – giving rise to unique fiber assemblies, i.e., aligned, porous, ribbon-like, hollow, helical, beaded fibers, which can greatly expand the complexity and subsequent potential of such biomaterials (3). As such, the structural diversity of electrospun materials have made them of prominence in several subfields of biomedical engineering and, in particular, tissue engineering (5), drug delivery (4), wound healing(6), and biosensing (7).

The electrospinning process represents an electro-fluid-dynamics problem, which stimulates electrified liquid jets to whip and elongate to form fine fibers (8). A standard laboratory-scale setup consists of four main components: a high-voltage DC (or AC) power supply, a syringe pump, a nozzle (usually metallic capillary), and a collector that can simply be a metallic foil/plate/disc (9).

During conventional electrospinning, electrostatic forces accumulated, by applying a high voltage to a polymer solution extruded through a nozzle-spinneret, induce a conically-shaped geometry referred to as the 'Taylor cone' at the nozzle's orifice. The repulsive electric forces overcome the surface tension of the polymer solution/melt, leading to vigorous whipping and splitting motions due to the bending instabilities generated, enabling a jet stream of fibers to travel towards a neutral (or oppositely charged) collector (10).

Considering that the production output of needle-based electrospinning devices is commonly meager, ranging at 0.01–0.3 g/h, scaling up the process has been progressively studied as a suitable approach to industrializing this fabrication process (10). Over the years, this was generally achieved by scaling up the spinneret's structure while retaining an energetically stable and well-distributed configuration. As opposed to multi-needle electrospinning, where the electric field around a given needle is affected by the nearby jets, which can produce inhomogeneous fibers, free-surface electrospinning is an alternative method capable of producing fibers at high-throughput with no constraints of clogged needles (11).

During nozzle-free electrospinning, the polymer solution is submerged in a bath containing a rotating cylinder electrode against a biased rotating collector electrode (12-14). By controlling the motor, the rotating speed of the roller can be changed. High-voltage power with a potential greater than 40 kV needs to be applied between the two rotating electrodes, which induces the formation of multiple Taylor cones emerging from the rotating electrode surface immersed in the solution bath (14, 15). When voltage is applied on the roller, the liquid changes to a conical shape and forms a significant number of Taylor cones (Figure 1) on the surface of the rotating spinneret. The roller electrospinning method has been proven to be a continuous and efficient process to fabricate NFs.

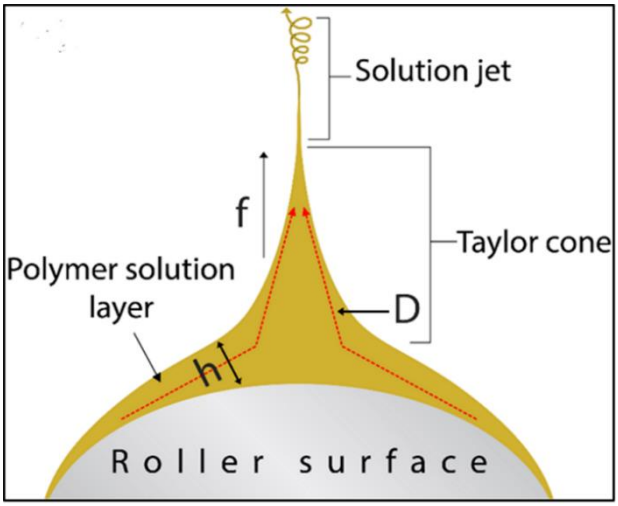

Figure 1. A schematic diagram of an open surface electrospinning Taylor cone formation, where *h* is the thickness of the layer, *D* is the diameter covered by the Taylor cone, and *f* is the electrostatic force

The concept behind free-surface electrospinning was initially described by Yarin and Zussman back in 2004 (16), and the self-organization of electrified liquid jets from an open flat surface was

mathematically delineated by Lukas et al. in 2008 (17), to date, research surrounding needleless electrospinning equipment accounts for less than 1.3% of the available literature. This could be possibly attributed to the high number of patents associated with free-surface electrospinning setups, as well as the extravagant costs of the commercially available equipment. For instance, products such as Nanospider™ (Elmarco, Ltd., Czech Republic) (18) an industrial-scale electrospinner, where a high-voltage potential (up to 80 kV) facilitates the formation of fibers out of a polymer-layered thread at a defined rate, cost anywhere between 170,000 to 300,000 USD (3,18). Ultimately the prevalence of conventional electrospinning prevents the clinical translation of several exciting and innovating advancements in the field, which present no real-world impact.

Our group's previous studies reported high production rates using rotating stainless steel and copper coil spinnerets. We have shown that the fiber production rate of the nozzle-free setup to that of a commercially available electrospinning device (IME, Netherland) using 7.5% (w/v) polycaprolactone (PCL) is an 11-fold higher (6). In a similar study, Wang et al. (19) indicated that hybrid nanoparticle-decorated chitosan NFs using a cylinder spinneret produced fibers at a 50 g/h rate instead of 0.02-1 g/h for the needle-based electrospinning device employed.

In a recent study by Agrawal and Pramanik (20), chitosan- poly(vinyl alcohol) blended nanofibrous scaffolds (with an average fiber diameter of 269 nm), formed using a needleless setup, were found to present good attachment, growth, and expansion in human mesenchymal stem cells. Keirouz et al. (5) and (6) employed the device developed to successfully electrospun PVP/poly(glycerol sebacate) (PGS) semi-transparent skin-like membranes with similar mechanical properties to anatomically variant skin regions, as well as silk fibroin-containing trinary composite microfibers incorporating PCL and PGS, which presented tuneable hydrophobicity. Radacsi et al. (21) utilized a similar needleless electrospinning device to fabricate nanoparticle-decorated poly(vinylpyrrolidone) (PVP) and polyaniline (PANI) NFs (average fiber diameter 123.9 ± 32 nm). Tan et al. (22) employed the nozzle-free electrospinning apparatus to develop carbonized electrospun polyacrylonitrile (PAN)/poly(acrylic acid) (PAA) for electrochemical sensing using precursor NFs containing iron oxide, gold nanoparticles, or reduced graphene oxide.

The technical note presented here describes the design and construction of a nozzle-free electrospinning apparatus that encompasses several configurations of spinnerets, collector assemblies, and solution reservoirs manufactured to optimize polymer efficient production of micro/-nanofibers. The cost-effective design provided, costing between 1500-2000 USD to assemble, can permit researchers to conduct lab-scaled research on high-throughput fiber production at a low cost.

2 Experimental section

A comprehensive list of the materials and components used to construct the nozzle-free electrospinning device is provided in Table S1. All the setup parts were designed using Solid Edge (v.2019, Siemens PLM Software, USA). The CAD files of the various components (in .par file format) are available for download at the journal's website.

3 Results and discussion

A rendered CAD model of the nozzle-free electrospinning equipment is depicted in Figure 2. The setup consists of five major sub-assemblies: (i) the spinneret, (ii) the collector drum, (iii) heating units, (iv) a three-layer lid, and (v) electronics. An exploded CAD model of the nozzle-free electrospinning setup can be found in Figure S1.

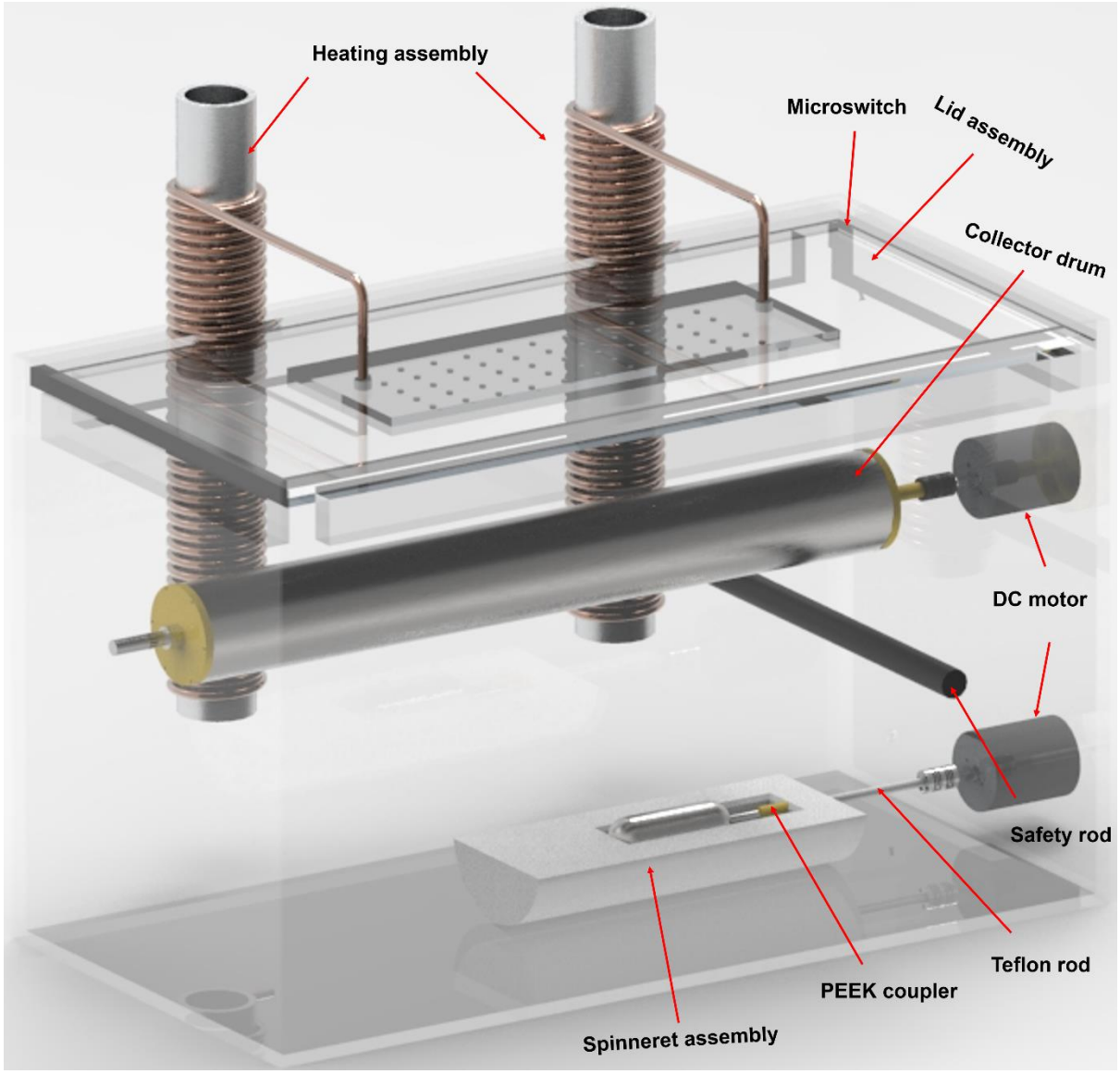

Figure 2. Rendered CAD model of the nozzle-free electrospinning setup with that description of each assembly and device component

3.1 Safety measures

As electrospinning uses high voltage to electrify the polymer solution and produce fibers, an electrically insulating material is required as a safety precaution. As glass presents a very high dielectric strength and resistivity, a low coefficient of thermal expansion, high tensile strength, and is transparent, it was chosen for the casing (23). For the casing of the electrospinning setup, a rectangular glass tank (aquarium) of 5 mm glass thickness (dimensions: 610 (length) x 308 (width) x 380 (height) mm) was used. In total, 13 holes were carefully drilled in various compartments of the glass aquarium using a

125 circular diamond-tipped drill bit hole saw and drill positioning tools, taking into account the fragility of
126 glass material.

127 A round plastic (polyoxymethylene; POM) safety rod was placed below and antiparallel to the
128 collector's direction as a safety measure to prevent direct contact between the negative and positive high
129 voltage connections, in the unlike scenario, the collector drum was to detach during the electrospinning
130 process due to high rotation speed.

131 At the top of the glass tank, four rectangular acrylic pieces were glued on, using epoxy, facing
132 inwards and parallel to each other, to support the placement of the lid. A safety interlock was mounted
133 on one of the rectangular acrylic pieces, at the midsection between the top of the aquarium and the lid
134 support, where the interlock (microswitch) was placed, allowing for the automatic shutdown of the high
135 voltage components and prevent the onset of high voltage at the absence of the lid.

136

137 **3.2 Fabrication of the spinneret assembly**

138 The spinneret configuration during free-surface electrospinning plays an imperative part towards the
139 fiber production output. The spinneret's size and geometry, along with the polymer solution properties,
140 ambient parameters, and applied voltage, will direct the number of the emerging Taylor cones from the
141 open surface. Wei et al. (24) found that the electric field intensity reaches the highest values at the ends
142 of the cylinder spinneret and decreases towards the center, which may hamper jet formation. Electric
143 field profile and intensity simulations using COMSOL have demonstrated that, although the highest
144 electric field profile is generated towards the center of an annular spinneret, the electric field intensity
145 is at least 5-fold higher at the edges.

146 In the setup, the spinneret is connected to a high voltage power supply via a high-voltage wire loop
147 and is partially immersed in a solution bath. As the spinneret slowly rotates, a thin film of the polymer
148 solution forms on the upper (open) side of the spinneret that is not immersed, allowing for the jetting
149 of fibers from multiple Taylor cones throughout its surface. There are three spinneret assemblies: a
150 cylinder, a ball, and a spiral coil described in this technical note Figure 3.

Selecting the appropriate material for the spinneret assembly is critical due to the corrosive nature of different solvents. Teflon, stainless steel, and polyether ether ketone (PEEK) are well-documented towards their resistant nature against common solvents (25). The spinneret assembly consisted of a Teflon bath, a solid stainless-steel cylinder, a Teflon rod, a PEEK coupler, an HV wire loop, and a 12 V DC gear motor.

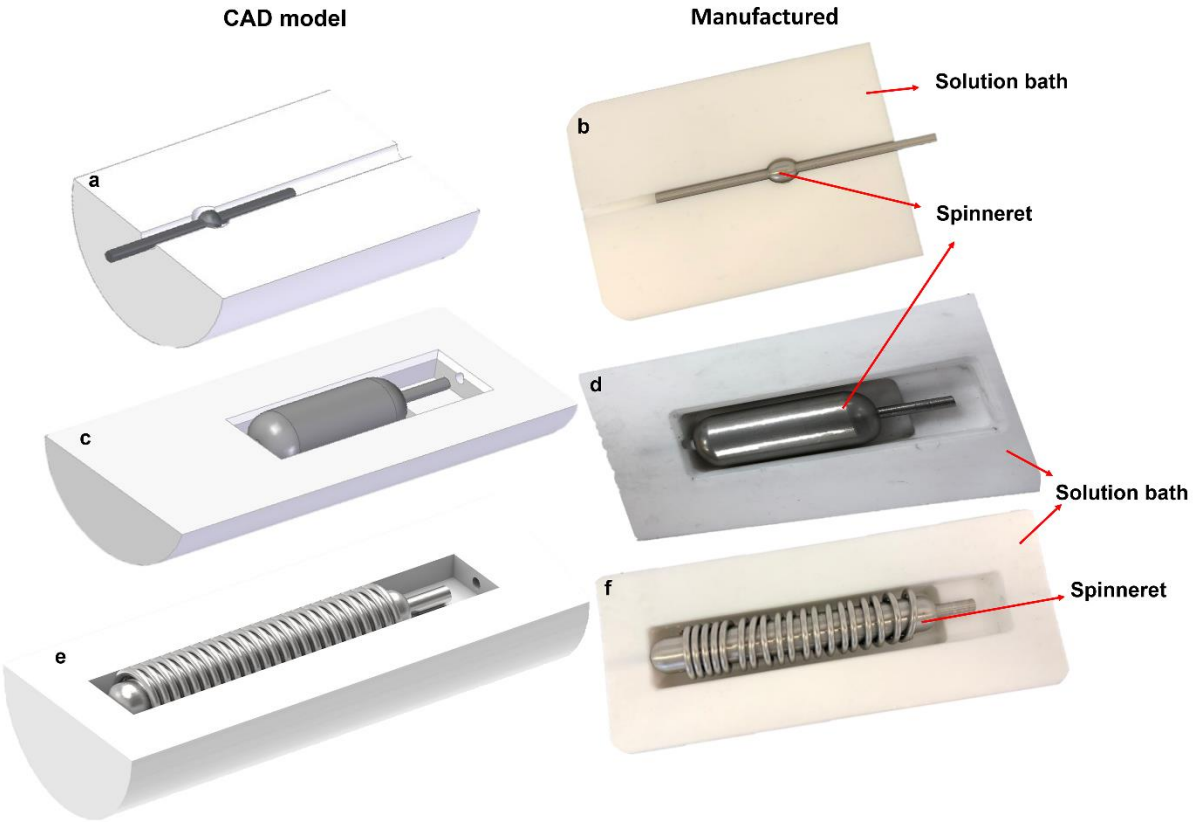

Figure 3. CAD models and corresponding photographs of the three spinneret assemblies. **(a-b)** CAD model and photograph of the small spherical spinneret, **(c-d)** CAD model and photograph of the medium-size spinneret, **(e-f)** CAD model, and a photograph of a large spinneret with the coil

The solution bath refers to the polymer reservoir within which the spinneret rotates. Three different solution baths were made to accommodate different solution volumes. The solution bath was machined from a Teflon rod stock to form a rectangular pot that can facilitate the electrospinning of polymer solutions.

The small Teflon bath (2 mL solution capacity) presents a 5.1 mm diameter semi-cylinder carved out along its length to facilitate the placement of the metallic rod that is used to rotate the spinneret Figure 3(a-b). The reservoir of16 mm in diameter and 8 mm in depth was carved in the shape of a semi-sphere out of the Teflon material to contain the polymer solution. The 2 mL Teflon bath was able to accommodate the immersion of a 10 mm stainless-steel metallic sphere, capable of rotating along its axis. A 5 mm round shaft attached to the metallic sphere ensured its straight horizontal position along the x-axis.

The medium solution bath was machined from a Teflon rod stock to form a rectangular pot that can facilitate the electrospinning of a 40 mL polymer solution (solution bath dimensions: 90 mm (length) × 30 mm (width) × 20 mm (depth)). A hole was drilled on the upper level of the rectangular pot to position the spinneret with a step for the shaft Figure 3(c-d). Then, a 6 mm opening was drilled on the Teflon bath, in which a small piece of Teflon rod mounted within the center (x-axis) of the metallic roller, ensured its straight positioning and subsequent ability to rotate. On the opposite side, a 6 mm opening drilled through the Teflon material allowed a 300 mm in length Teflon rod and a PEEK coupler to connect the spinneret with the DC motor. The device was designed to facilitate a stainless-steel metallic roller spinneret (113 mm (length) x 30 mm (width)). The metallic roller has tapered edges to prevent concentrated high electric fields from forming. An exploded CAD model of medium spinneret can be found in Figure S2.

The solution bath, within which the spinneret was submerged, provided a 5% margin on each side of the spinneret to allow for its rotation and polymer coating, and a 10% margin on the coupler-rod side for the positioning of the HV loop. Allowing minimal exposure of the polymer solution is an important aspect of the device, which provides shelter to volatile solvents and allows consistency throughout the electrospinning process.

The large spinneret assembly (60 mL solution capacity), conceptually similar to the 40 mL solution bath, was machined from a Teflon rod stock to form a rectangular cavity with a step for the shaft. As shown in Figure 3(e-f), the spinneret of the large assembly, a stainless-steel metallic roller, consisted of a solid stainless-steel spindle spiral stainless-steel coil is welded around it. The stainless-steel roller's

192 total length was 185 mm, where the diameter along the spiral coil was 21 mm. The spiral coil geometry
193 can increase the number of Taylor cones forming along the spinneret's surface due to the increased
194 curvature that leads to a stronger electric field than the smooth spinneret used in the medium Teflon
195 bath. An exploded CAD model of a large spinneret can be found in Figure S3.

196

197 **3.3 Fabrication of the collector assembly**

198 The collector was manufactured from a stainless-steel cylinder to attain good electrical conductivity
199 and charge distribution along its surface (15). The collector assembly consisted of five distinct parts: a
200 hollow stainless-steel cylinder, two PEEK discs for the positioning of the cylinder, and two protruding
201 shafts. Four 20 mm holes on the side of the collector allowed for the insertion of dry ice. The PEEK
202 discs were fixed on the hollow cylinder by six stainless steel screws, while the shafts were mounted on
203 the discs using two stainless steel screws for each Figure S4.

204 Cryogenic electrospinning is a technique that uses a sub-zero (in °C) temperature collector to
205 facilitate the simultaneous formation of nanofibers and ice crystals. The scaffold's pore size can be
206 adjusted from 10–500 μm, depending on various controllable factors, such as size and the amount of
207 ice crystals. The ice crystals are then removed by freeze-drying the fibrous scaffolds, leaving large void
208 spaces, which create an ultra-porous biomaterial with wide pores that can permit cell infiltration (10).

209 The cryo-collector assembly has a diameter of 64 mm and is 500 mm long Figure (4a-b). The shaft
210 connecting the collector to the electric motor was made out of PEEK Figure (4c-d) to avoid electrical
211 charges escaping from the collector's surface towards the DC motor. On the opposite side, an aluminum
212 shaft Figure 4(e-f) was inserted in the center of a 10 mm-diameter metallic ball bearing, allowing its
213 rotation.

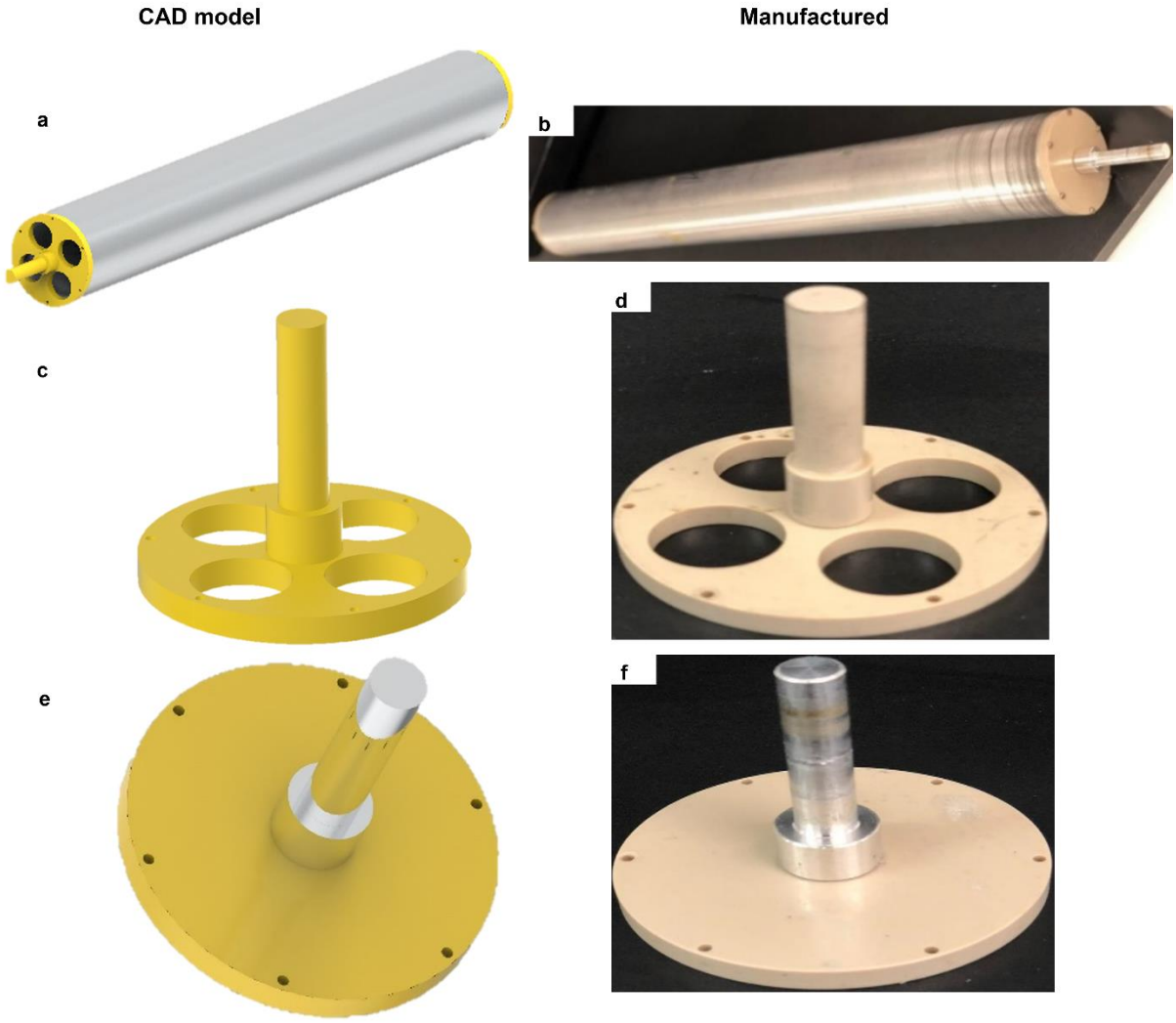

Figure 4. CAD model of the cryo-collector assembly **(a-b)** CAD model and photograph of the manufactured cryo-collector assembly **(c-d)** CAD model and photograph of the PEEK disc with four holes with the PEEK shaft **(e-f)** CAD model and photograph of the closing PEEK disc and aluminum shaft.

3.4 Heating and lid assembly

The lid assembly consisted of three rectangular glass plates, as shown in Figure 5(a-e). The ambient humidity is a critical factor that can directly affect the electrospinnability of a polymer solution, as well as the subsequent morphology of the fibers. For instance, high humidity can affect the morphology of the fibers by forming defects (e.g., beads), secondary morphologies (e.g., net-like spider webs), or by

completely halting a solution from being electrospun. The layered glass assembly allows the uniform distribution of gas (hot air, nitrogen) onto the collector assembly, controlling the humidity and temperature within the electrospinning chamber. Each rectangular glass plate was 590 mm (length) x 295 mm (width) x 5 mm (thickness). The outermost glass layer had 55 holes of 3 mm diameter arranged at five rows and 11 columns, similar to a perforated glass. This allowed for the uniform distribution of air/nitrogen across the glass aquarium, at a constant flow across the holes. A rectangular glass piece was cut out from the middle glass plane at the same position where the 55 holes were presented on the bottom glass plane to allow for the gas distribution and circulation. The top glass plane presented two openings for Swagelok tube fittings from where copper tubing linked to the gas supply was connected to the lid. Heavy-duty suction cups were positioned to lift the lid.

Controlling the electrospinning chamber temperature, by heating the gas was achieved by using two heating assemblies positioned outside the glass aquarium. The heating assembly consisted of a heat sink, made of an aluminum pipe (50 mm (inner pipe diameter) x 400 mm (length)). Then, 6 mm copper tubing was used to wrap the heat sink, as shown in Figure 5(f). Wrapping the aluminum pipes using high-temperature heating and insulation tapes, prevent heat loss to the environment. Two metallic hose clamps were used to stabilize the assembly and hold it together, as shown in Figure 5(g). The high-temperature insulating tapes were heated by an MC 242 electric heating controller.

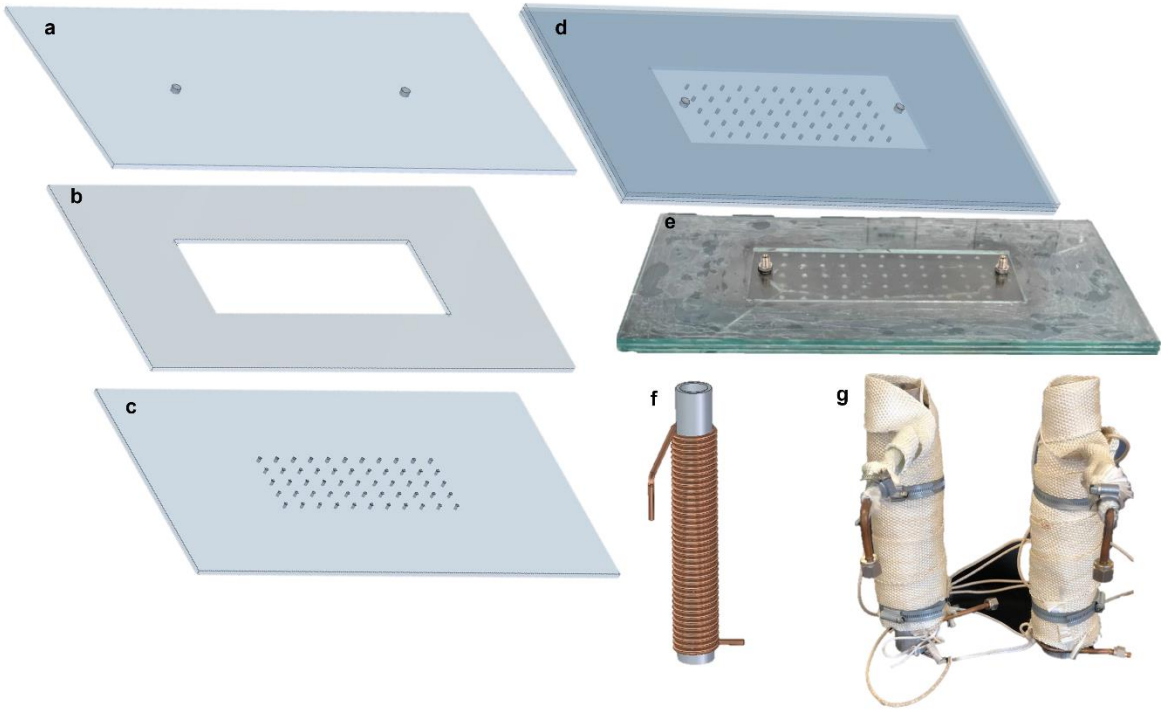

Figure 5. CAD model of the glass lid and heating assembly. **(a)** CAD model of top glass plane, **(b)** CAD model of middle glass plane with the rectangular cutout **(c)** CAD model of bottom glass plane with 55 holes, **(d)** CAD model and **(e)** photograph of complete 3-layer lid assembly, **(f)** CAD model of the heat sink with the copper coil wrapper around it **(g)** photograph of heating assembly

3.5 Electronics

Two high-voltage DC power supplies (Information Unlimited, New Hampshire, USA) of adjustable output voltage, one of negative and one of positive voltage output, were utilized to electrify the polymer solution and draw the fibers towards the collector. Both have the capability to be adjusted between 5-35 kV, allowing the users to set a total potential difference of up to 70 kV between the rotating collector and the spinneret.

The rotations of the spinneret and the collector are independently controlled by DC motors. The spinneret rotational speed is constant, controlled by a direct current, 6 V at 5 revolutions per minute (rpm) when no load is coupled to the shaft. The collector is fitted with a brushed DC motor rated at

4500 rpm when unloaded (Bosch, Germany). The user can adjust the effective rpm utilizing two controlling mechanisms; a speed controller and a DC source feeding the circuit.

The speed controller module used with the proposed setup (Model EM-185, Electromen OY, Finland) regulates the effective voltage fed to the motor, enabling the user to set the rotation of the collector from an estimate of 100 rpm up to its rated maximum rpm value, when no load limitation due to weight is considered. This controller supports only coarse rpm adjustments and will not allow the user to reliably set speeds below 100 rpm. The module can be powered up by any DC source that provides 12-24 V DC, and it can safely source up to 3 A to the motor. Identifying the maximum current that the module can handle is important for the design since the setup is required to operate under heavy load conditions when the hollow collector is filled with dry ice in the cryo-electrospinning mode. In this case, a higher current spike is required by the motor for initiating rotation, which can be easily covered by the 3A limit outlined for the selected speed controller.

The power source selected for powering up the collector motor and its control circuit is an adjustable DC power supply (Model HCS 3102, Manson Engineering Industrial Ltd.) with programmable output voltage and current. The user can select an output voltage between 0 and 30 V in 0.1 V increments and an output current between 0 and 5 A with 0.1 A increments. The selected source supports constant current and constant voltage supply modes. Users will typically employ the constant voltage supply mode, which will provide the requested voltage to the load while keeping it constant but allows variations in the supplied current.

3.6 Fabrication of nanofibers

The current nozzle-free electrospinning setup was successfully used to produce NFs using different polymers. The SEM images of these electrospun NFs are shown in Figure 6 (a-f). The nozzle-free electrospinning setup can produce homogenous and uniform electrospun mats over a large area. The higher production rate of electrospun fibers can be achieved in very short time, 1.45 g of nanofibers collected on an aluminum foil in just 18 minutes, as shown in Figure 6 (g).

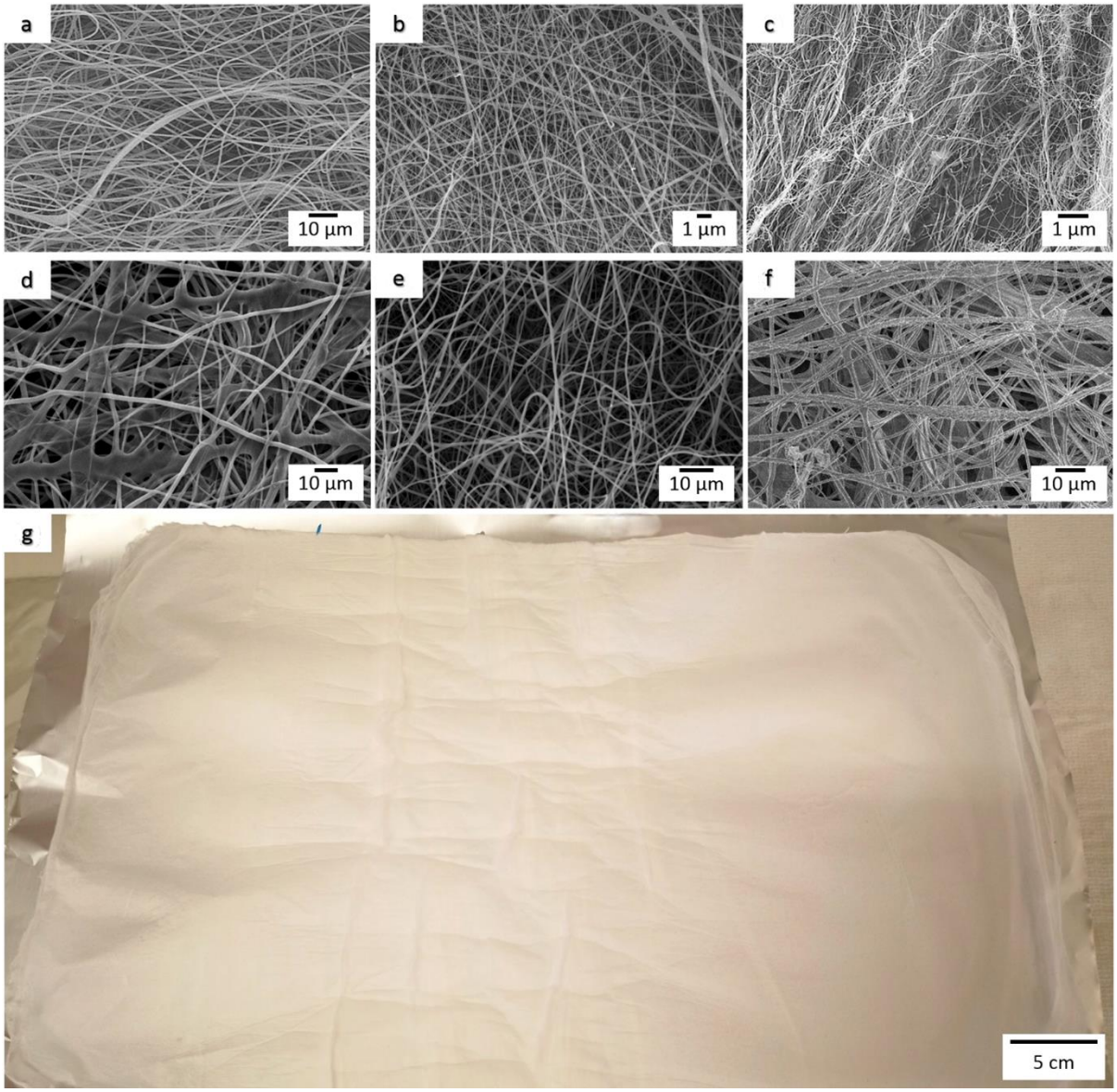

Figure 6. Nozzle-free electrospinning setup used to produce electrospun fibers using different polymers **(a)** Polyvinylpyrrolidone in N, dimethylformamide (DMF)/Ethanol/distilled water **(b)** polycaprolactone in trifluoroacetic acid **(c)** silk fibroin dissolved in trifluororethylene **(d)** polyaniline / polyacrylic acid in DMF **(e)** polyacrylonitrile in DMF **(f)** polyvinylidene fluoride/polyethylene glycol in DMF/distilled water **(g)** polyvinylidene fluoride/polyethylene glycol composite material electrospun directly on an aluminum foil. The electrospun mat shown in Figure 6(g) was obtained within 18 minutes of electrospinning

4 Conclusion

Nozzle-free electrospinning is a promising technology for large-scale production of NFs, as free-surface electrodes are not associated with clogging issues and nonuniform electric field distribution, allowing for the formation of multiple Taylor cones across the spinneret's surface. This technical note presents a step-by-step guide for the fabrication of a low-cost, temperature-controlled, nozzle-free electrospinning setup. The setup includes a cryo-collector, which enables cryo-electrospinning for obtaining ultra-porous materials. Three different spinnerets of variable size and geometries allow different solution volumes to be accommodated. A multi-channel gas lid allows uniform gas circulation, counter to the electrospinning direction, capable of controlling the humidity and temperature, which directly affects the solvent evaporation rate. As indicated, this setup has been successfully tested using several polymers and solvent systems and can be further validated by published works in the fields of drug formulation (4), tissue engineering (5), and wound healing (6). By utilizing this setup, high-throughput production of fibers can be achieved efficiently and at a low cost that can benefit the advancement of electrospun materials in health care, energy, and a wide range of industrial sectors.

Acknowledgments

The authors would like to thank Andrew Mullen, Paul Aitken, and Fergus Dingwall of The University of Edinburgh for their help and support. We would also like to thank Michael Chung for his valuable input to improve the image quality.

Conflict of interest

None.

Funding

The authors would like to acknowledge the School of Engineering of the University of Edinburgh for funding through the McCann Prize (grant number: 100-IRMI/INT 16/6/2 (010/2017)). The first author would like to express thanks to Higher Education Commission (HEC), Pakistan, for their financial support.

Availability of supporting data

Table S1 provides information and the suppliers for all the materials used to assemble the nozzle-free electrospinning device. The CAD and part files (.Par file format) can be downloaded at no cost.

Ethical Approval: Not required

References

1. Wang C, Wang J, Zeng L, Qiao Z, Liu X, Liu H, et al. Fabrication of Electrospun Polymer Nanofibers with Diverse Morphologies. Molecules. 2019;24(5).
2. Rahman NA. Electrospun conducting polymer nanofibers for biomedical applications: University of Auckland; 2012.
3. Bhardwaj N, Kundu SC. Electrospinning: a fascinating fiber fabrication technique. Biotechnol Adv. 2010;28(3):325-47.
4. Keirouz A, Radacsi N, Ren Q, Dommann A, Beldi G, Maniura-Weber K, et al. Nylon-6/chitosan core/shell antimicrobial nanofibers for the prevention of mesh-associated surgical site infection. J Nanobiotechnology. 2020;18(1):51.
5. Keirouz A, Fortunato G, Zhang M, Callanan A, Radacsi N. Nozzle-free electrospinning of Polyvinylpyrrolidone/Poly(glycerol sebacate) fibrous scaffolds for skin tissue engineering applications. Med Eng Phys. 2019;71:56-67.
6. Keirouz A, Zakharova M, Kwon J, Robert C, Koutsos V, Callanan A, et al. High-throughput production of silk fibroin-based electrospun fibers as biomaterial for skin tissue engineering applications. Materials Science and Engineering: C. 2020.
7. Tan E, Pappa AM, Pitsalidis C, Nightingale J, Wood S, Castro FA, et al. A highly sensitive molecular structural probe applied to in situ biosensing of metabolites using PEDOT:PSS. Biotechnol Bioeng. 2020;117(1):291-9.
8. Kong T, Stone HA, Wang L, Shum HC. Dynamic regimes of electrified liquid filaments. Proc Natl Acad Sci U S A. 2018;115(24):6159-64.
9. Keirouz A, Chung M, Kwon J, Fortunato G, Radacsi N. 2D and 3D electrospinning technologies for the fabrication of nanofibrous scaffolds for skin tissue engineering: A review. Wiley Interdiscip Rev Nanomed Nanobiotechnol. 2020;12(4):e1626.
10. Niu H, Lin T. Fiber Generators in Needleless Electrospinning. Journal of Nanomaterials. 2012;2012:1-13.
11. Williams GH R-AB, Luo C. Moving from bench to the clinic. Nanofibres in Drug Delivery. London, UK: UCL Press; 2018.

12. Haitao Niu XW, Tong Lin. Upward Needleless Electrospinning of Nanofibers. Journal of Engineered Fibers and Fabrics. 2012.
13. Niu H, Wang X, Lin T. Needleless electrospinning: influences of fibre generator geometry. Journal of the Textile Institute. 2012;103(7):787-94.
14. Niu H, Wang X, Lin TJJoef, fabrics. Upward needleless electrospinning of nanofibers. 2012;7(2_suppl):155892501200702S03.
15. Niu H, Lin T, Wang X. Needleless electrospinning. I. A comparison of cylinder and disk nozzles. Journal of Applied Polymer Science. 2009;114(6):3524-30.
16. Yarin AL, Zussman E. Upward needleless electrospinning of multiple nanofibers. Polymer. 2004;45(9):2977-80.
17. Lukas D, Sarkar A, Pokorny P. Self-organization of jets in electrospinning from free liquid surface: A generalized approach. Journal of Applied Physics. 2008;103(8).
18. Elmarco. Elmarco Laboratory equipment 2020, February 19 [Available from: https://www.elmarco.com/laboratory-equipment.
19. Wang L, Zhang C, Gao F, Pan G. Needleless electrospinning for scaled-up production of ultrafine chitosan hybrid nanofibers used for air filtration. RSC Advances. 2016;6(107):105988-95.
20. Agarwal T, Narayan R, Maji S, Behera S, Kulanthaivel S, Maiti TK, et al. Gelatin/Carboxymethyl chitosan based scaffolds for dermal tissue engineering applications. Int J Biol Macromol. 2016;93(Pt B):1499-506.
21. Radacsi N, Campos FD, Chisholm CRI, Giapis KP. Spontaneous formation of nanoparticles on electrospun nanofibres. Nat Commun. 2018;9(1):4740.
22. Tan HL, Sanira Putri MK, Idris SS, Hartikainen N, Abu Bakar NF, Keirouz A, et al. High-throughput fabrication of carbonized electrospun polyacrylonitrile/poly(acrylic acid) nanofibers with additives for enhanced electrochemical sensing. Journal of Applied Polymer Science. 2020;137(43).
23. N.A. Othman MAMP, Z. Adzis, H. Ahmad, N.A. Ahmad, H. Kamarden, A.A. Suleiman. Characterization of charge distribution on the high voltage glass insulator string. Journal of Electrostatics. 2014;72(4):315-21.
24. Wei L, Sun R, Liu C, Xiong J, Qin X. Mass production of nanofibers from needleless electrospinning by a novel annular spinneret. Materials & Design. 2019;179.
25. Zhou W, Zhang W, Liu Y, Yu X, Chen Z. Polydopamine-functionalized poly(ether ether ketone) tube for capillary electrophoresis-mass spectrometry. Anal Chim Acta. 2017;987:64-71.

Figure 2

Click here to access/download;Figure;Figure 2.tif

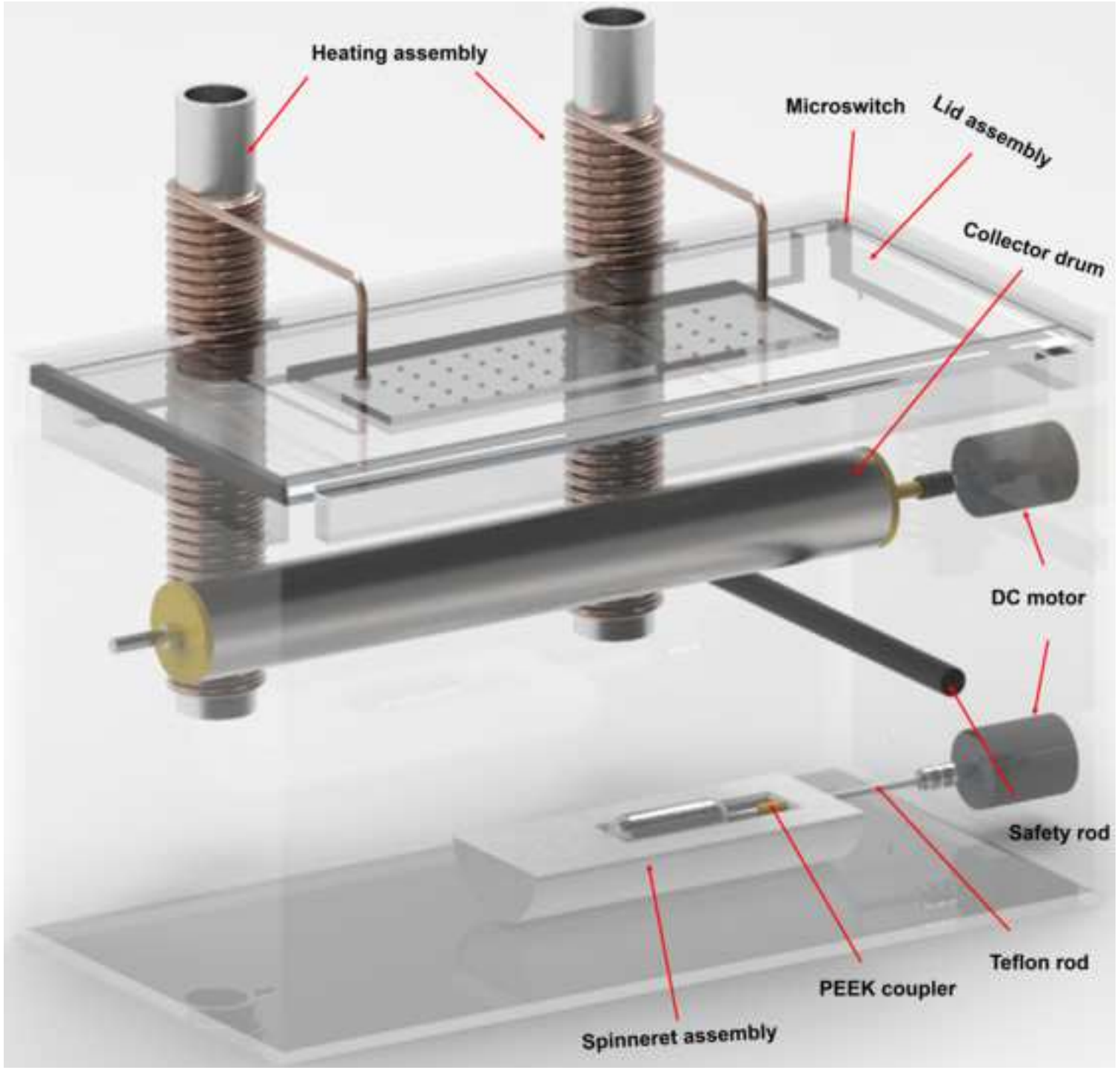

Figure 3

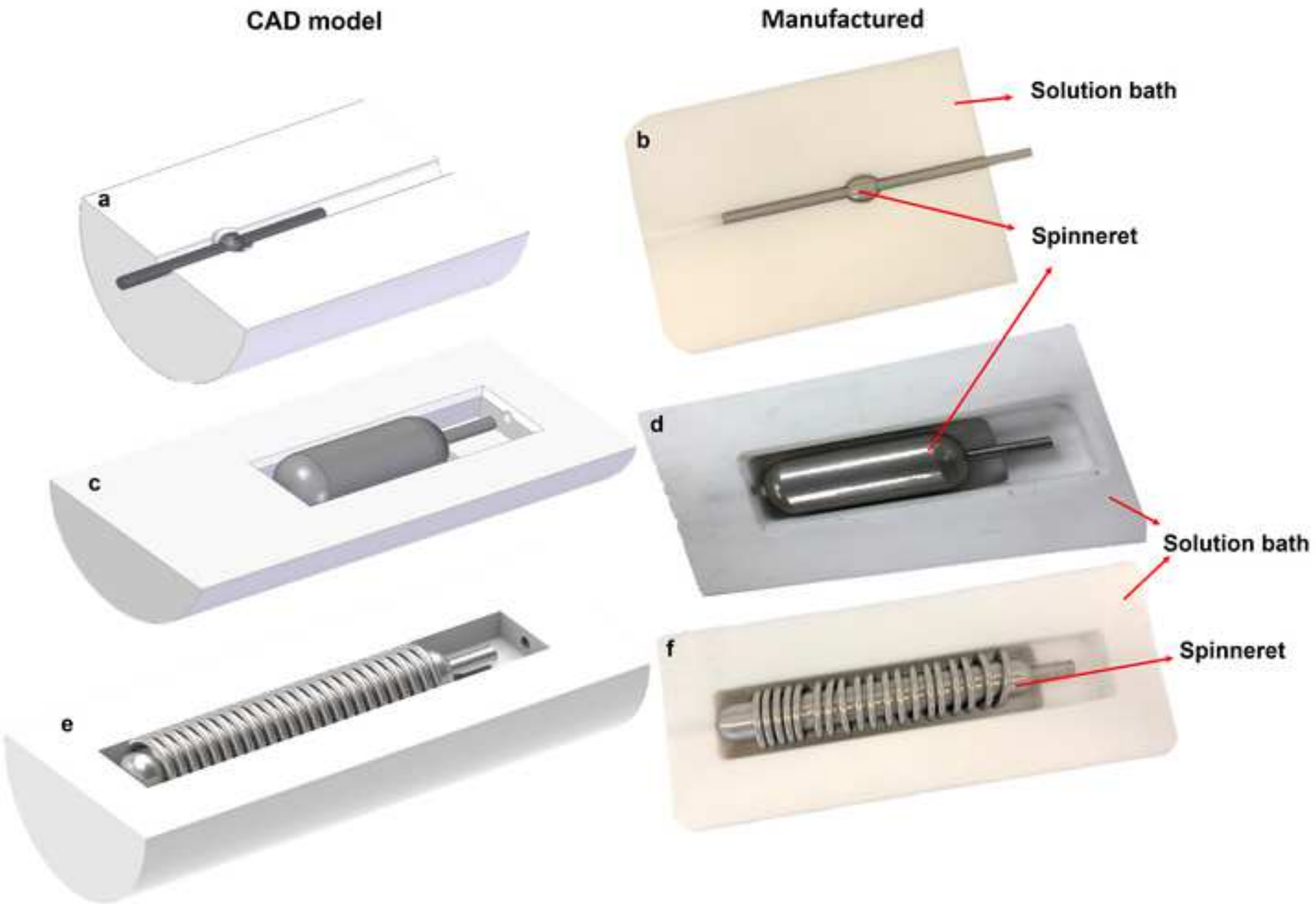

Figure 4

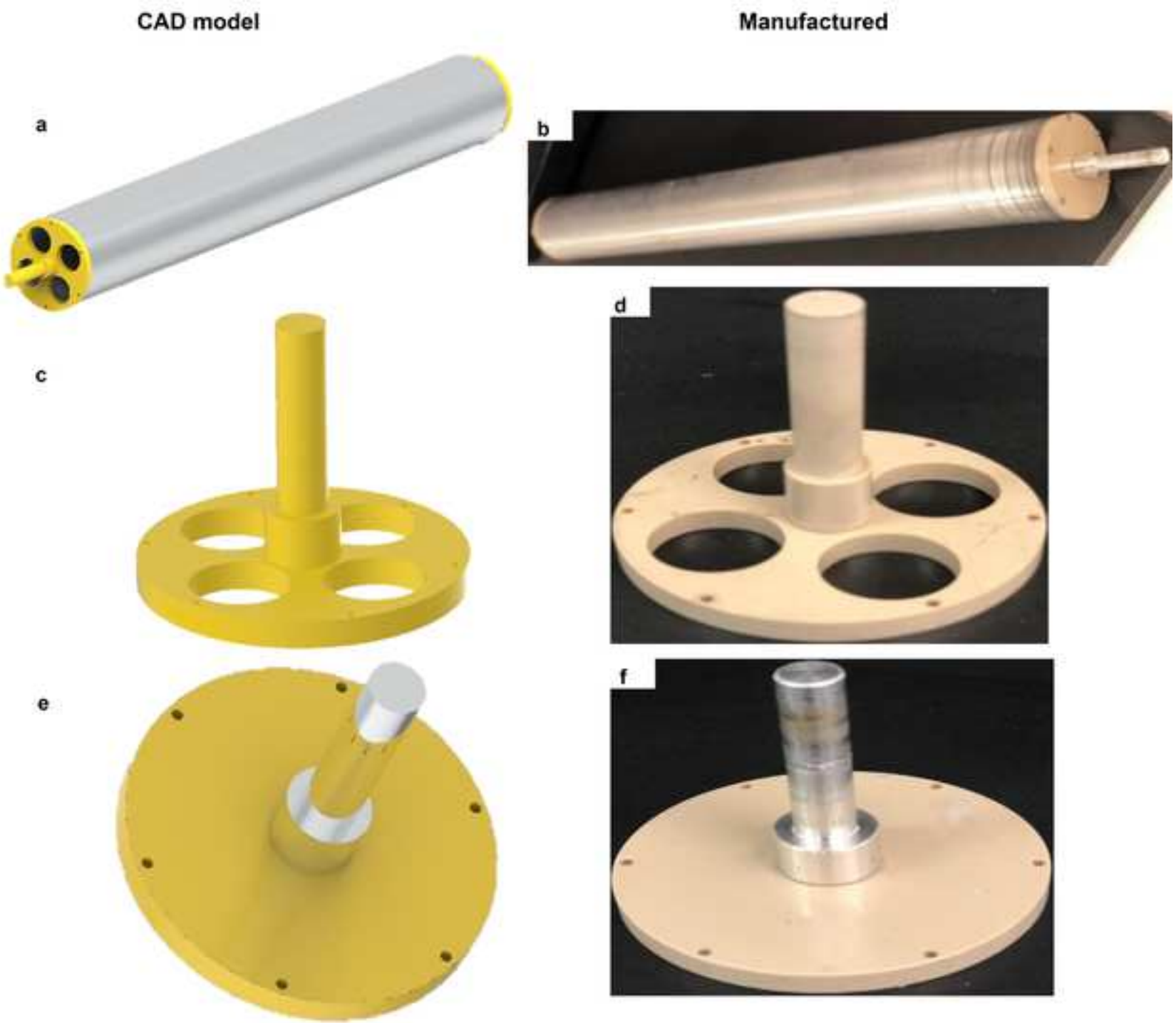

Figure 5

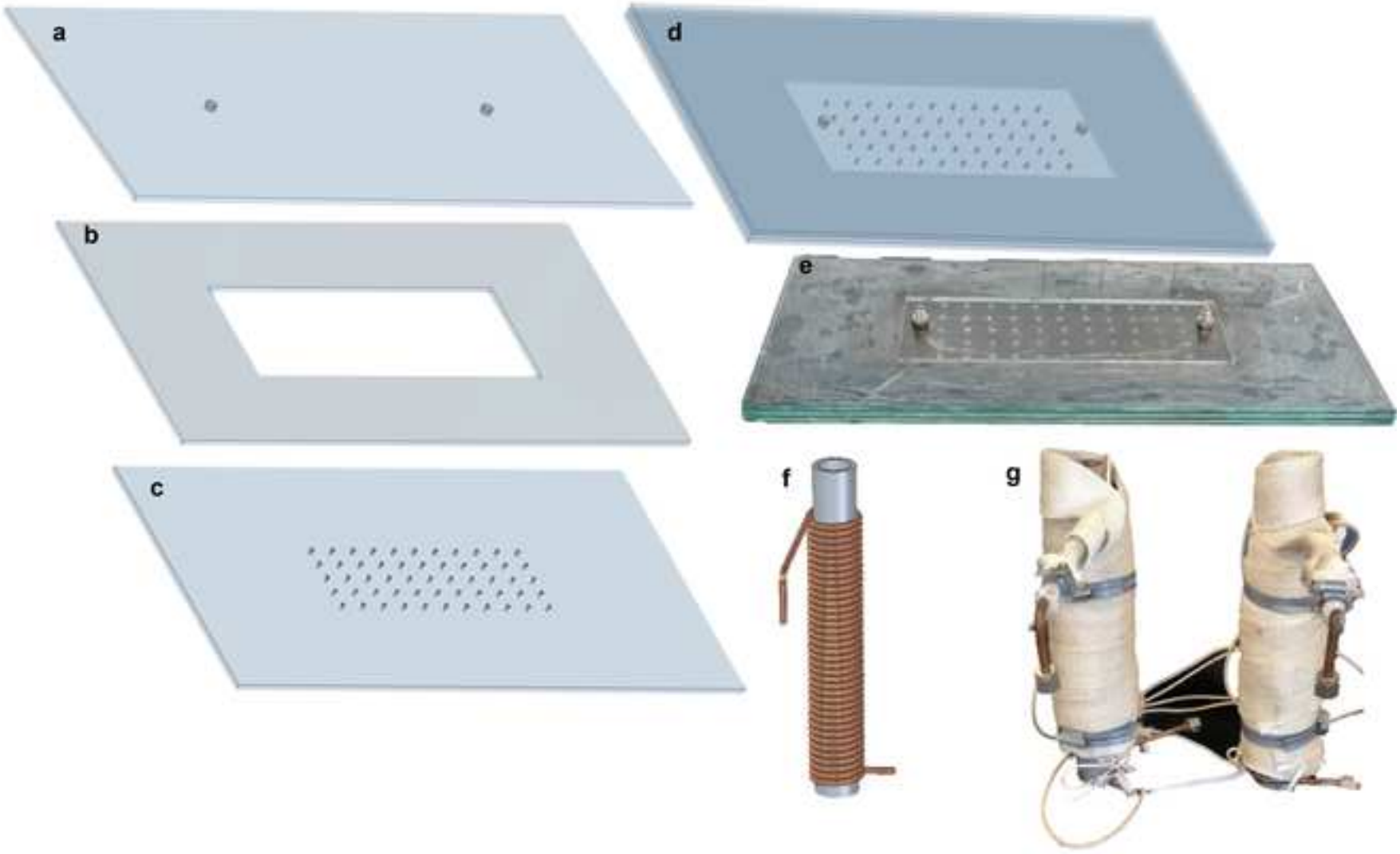

Figure 6

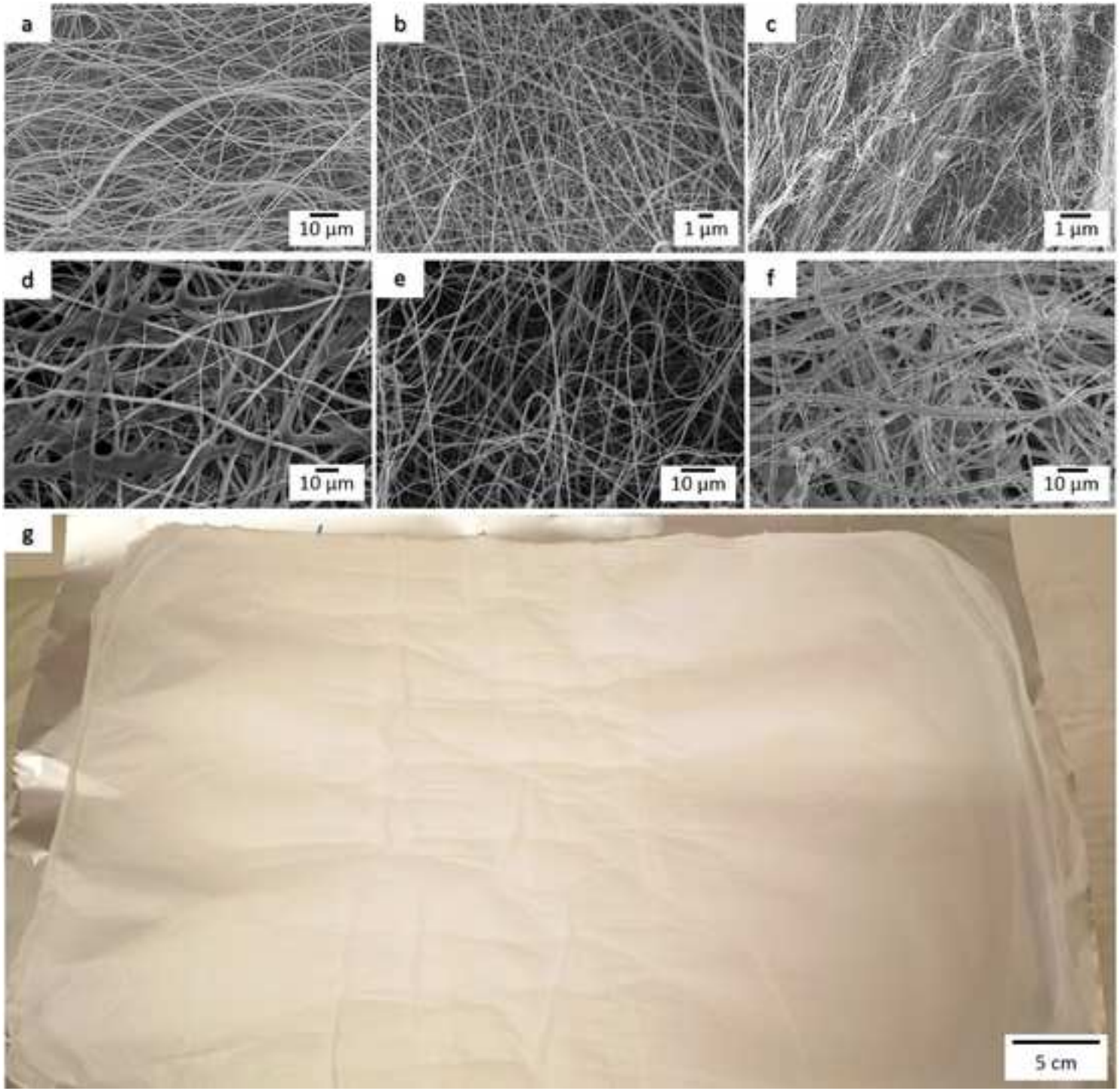

Figure 1

Click here to access/download;Figure;Figure_1.tif

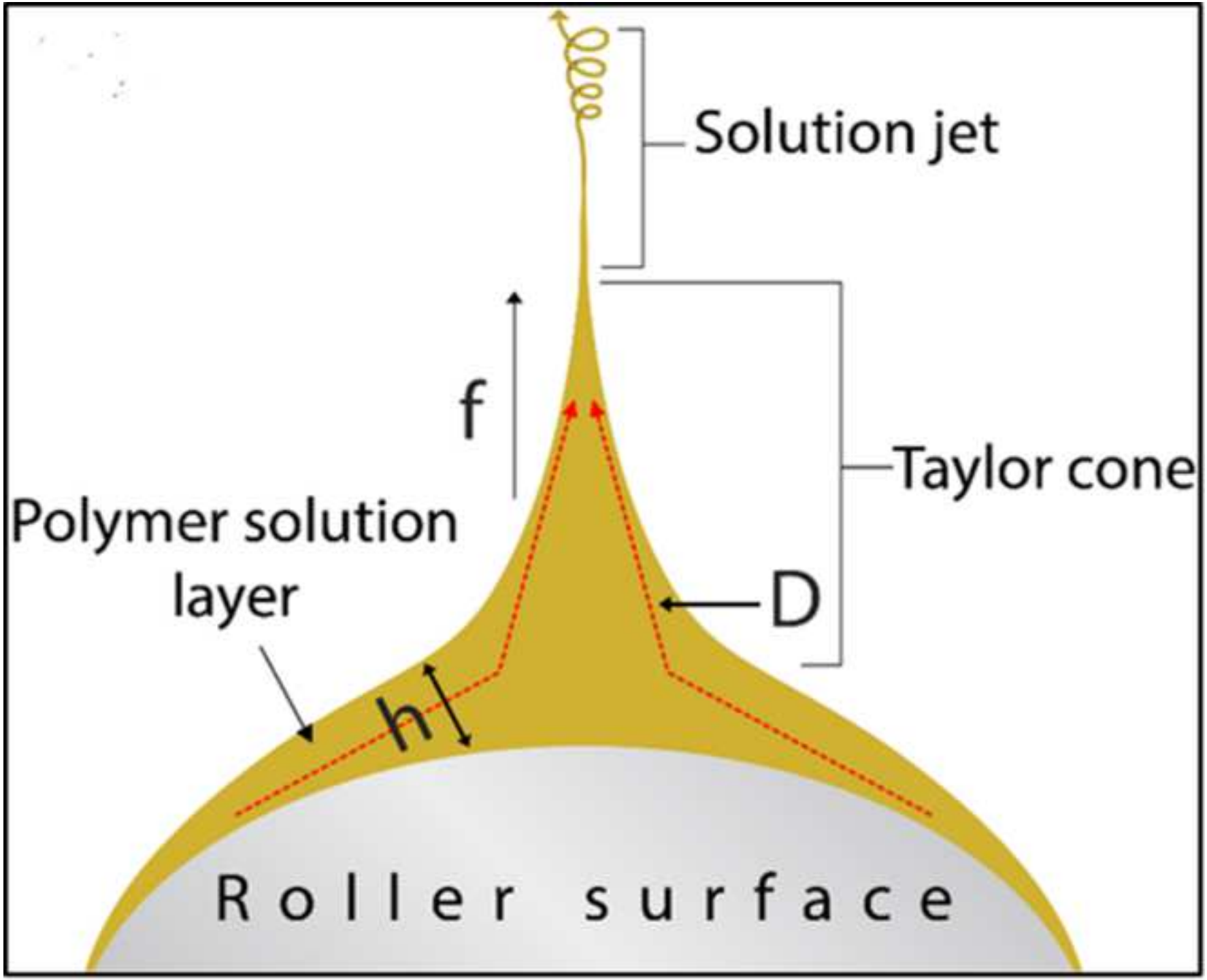

Click here to access/download

Supplementary data

Supplementary data.docx

Drawings

Click here to access/download

Supplementary data

Drawings.rar

S2

Click here to access/download
Supplementary data
S2.tif

S3

Click here to access/download

Supplementary data

S3.tif

S4

Click here to access/download

Supplementary data

S4.tif